17th World Conference on Earthquake Engineering, 17WCEE
Sendai, Japan - September 13th to 18th 2020

EXPERIMENTAL INVESTIGATION OF HYSTERETIC PERFORMANCE OF SELF-CENTERING VARIABLE FRICTION DAMPER BRACE

YW. Wang[1], Z. Zhou[2], KS. Zhao[3]

[1] *Nanjing, China, Southeast Univ., Key Laboratory of Concrete and Prestressed Concrete Structures of the Ministry of Education*
e-mail address: klxzwyw@qq.com

[2] *Nanjing, China, Southeast Univ., Key Laboratory of Concrete and Prestressed Concrete Structures of the Ministry of Education*
e-mail address: seuhj@163.com

[3] *Nanjing, China, Southeast Univ., Key Laboratory of Concrete and Prestressed Concrete Structures of the Ministry of Education*
e-mail address: sozhso@163.com

Abstract

In the design of traditional aseismic structural systems, frame structures suffer controlled ductile inelastic response to dissipate energy by allowing a high degree of plastic deformation under earthquake. However, under repeated inelastic action and residual deformations, structural systems sustain damage which is difficult to repair or cost greatly after earthquake. To improve this drawback of traditional energy dissipation system, self-centering variable friction damper (SC-VFD), as a novel bracing system, providing larger post-yield stiffness and energy dissipation, can effectively improve the reparability of the structure after a strong earthquake. In this paper, the concept and working mechanism of SC-VFD brace was firstly mentioned and introduced. Then, theoretical analysis of variable stiffness and sliding force of VFD system as well as SC-VFD brace was conducted. Finally, quasi-static experiments on VFD braces and SC-VFD braces was conducted and carried out. The theoretical analysis and experimental results show same tendency, describing the reliability and feasibility of SC-VFD braces. Moreover, the SC-VFD brace depicted a normal flag-shape hysteresis curve at flat part while a novel flag-shape at slope part with another activation and larger post yield stiffness. The residual displacements are smaller than 0.1% drift and confirm good self-centering capability under cyclic loading protocols.

Keywords: Self-centering; Variable friction damper; Hysteretic performance; Energy dissipation; BFRP;

1. Introduction

In traditional structural designing, the structure have to suffer from larger plastic deformation to dissipate energy to guarantee the safety of structure [1]. However, these structure are difficult to repair due to larger inelastic deformation and serious damage after earthquake. So the concept of resilient structures is proposed and leads to a tendency of earthquake researching from earthquake resistance to resilience. Resilience is defined that the structure can quickly restore their function with simple repair or without any repair. Obviously, traditional structures cannot satisfy the requirement of resilience and clearly, the self-centering energy dissipation brace (SCED) brace, is an effective method to reduce the residual displacement and damage of structures.

The SCED brace was firstly proposed in structures by using disc springs to provide restoring force and friction force to provide energy dissipation and this braces showed a clear flag-shape hysteresis curve [2, 3]. Furthermore, it's become more popular to use the shape memory alloy (SMA) or composition tendons [4-6] to contribute the self-centering function while the bucking restrained brace (BRB) or all-steel bamboo-shaped energy dissipaters to contribute the energy dissipation. They all show obvious flag-shape hysteresis curve and less residual displacement, depicting a good self-centering phenomena. However, the stiffness and strength of these materials will decrease sharply and these types of braces are easily failed or broken after earthquake [7]. To solve this problem, friction energy dissipation dampers, as one of the most effective passive dampers components with stable and predictable hysteresis curves and higher reuse ratio, are widely accepted in construction of structures. Based on former research, non-asbestos organic (NAO), a type of non-metallic material, with mitigated loss of sliding force and perfect wear-resisting properties, has been found and introduced [8]. Meanwhile, in order to achieve the larger post-yield stiffness and energy dissipation, a novel friction dissipation brace, by combining pretensioned BFRP tendons for self-centering function and variable friction damper (VFD) for energy dissipation, was invented [9-13].

In this paper, the concept and working mechanism of SC-VFD brace was firstly mentioned. Then theoretical analysis of variable post-yield stiffness and sliding force of VFD system and SC-VFD brace was carried out. Finally, based on the theoretical analysis, VFD brace without BFRP and SC-VFD brace were designed and corresponding quasi-static tests were performed and compared with the theoretical results.

2. Mechanism of SC-VFD Brace

As shown in the Fig. 1, the SC-VFD brace mainly includes two parts: the self-centering system used to providing the restoring force and two friction dampers at each side of brace used to providing the energy dissipation.

The self-centering system, which mainly includes the BFRP tendons, the inner tube, outer tube and end plates, can force the brace back to initial position after the deformation under earthquake. In order to achieve the self-centering function, the BFRP tendons, which have ability of relatively high elastic elongation, are firstly prestressed. Lengths of inner tube and outer tube are equal under the ideal condition. Firstly, the inner tube is placed in the outer tube while the BFRP tendons s is placed in the inner tube without any connection. Then the two end plates are placed at the two end of inner tube and outer tube and the section of end plates are larger than inner tube and outer tube. Moreover, the BFRP tendons are pretensioned to provide initial self-centering force and

bolted by left and right end plates. Meanwhile, initial pretensioned force in BFRP tendons would eliminate some gaps between two ends of tubes and two end plates.

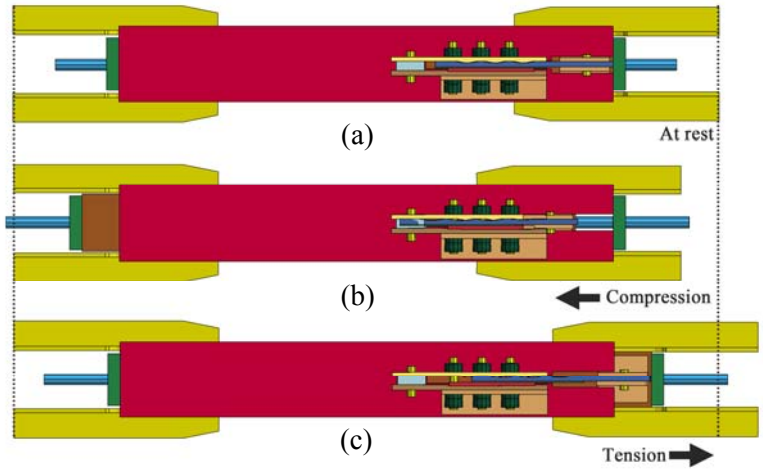

Fig. 1 – The concept and working mechanism of SC-VFD braces

The VFD system is assembled by grooved top steel plate (GTSP), grooved middle steel plate (GMSP), grooved bottom steel plate (GBSP), NAO friction pad and stainless plate, combinations of pre-stressed disc springs (Belleville spring) and several high-strength bolts. Meanwhile, it can provide the variable friction force, two activation and larger post-yield stiffness. The GMSP is bolted with inner tube while the GBSP is bolted with outer tube firstly. Through the grooves with angle, the bottom of GTSP and top of GMSP is assembled and machined (Fig. 2). The grooves is made by consecutive flat and slope parts, and the flat parts of convex portion are shorter than concave portion so that there is a flat slide distance L between GTSP and GBSP. Moreover, the NAO pad is assembled with the GBSP through the groove of GBSP because the length and wide of groove is exact with the NAO pad while the high of groove is smaller than NAO pad, guaranteeing the no sliding distance between GBSP and NAO pad. Then the stainless plate is welded at the bottom of GMSP. Finally, GTSP and GBSP are bolted and clamped in a manner so that NAO pad and combination of GMSP and stainless plate are sandwiched by two cap plates.

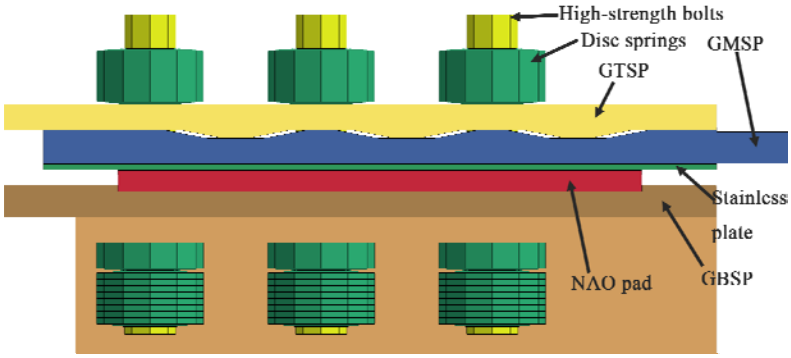

Fig. 2 – The concept of VFD system

Based on the construction of GTSP and GMSP, the stage of sliding can be divided into two different process. Firstly, when the sliding distance is smaller L [Fig. 3(a) and (b)], GTSP and GBSP are sliding at the flat part without any gap opening, which is perpendicular to horizontal sliding direction D. There is no deformation of disc springs and the pre-stressed clamping forces

keep as constant. Therefore, the friction force between GTSP and GMSP, between stainless plate and NAO pad remain as a constant value. With the increasing of external displacement and when the sliding distance is larger than L [Fig. 3(a) and (c)], GTSP and GMSP are sliding at slope part, causing a gap opening δ, which is perpendicular to horizontal sliding direction D. Meanwhile, the combination of disc springs is compressed and provides larger clamping force in friction blots. Thus, with the increasing clamping force, the friction between GTSP and GMSP, between stainless plate and NAO pad increase reversely. Therefore, the reasonable angle of groove and the sufficient deformation of disc spring is curial to SC-VFD brace, especially when the brace slides at slope part.

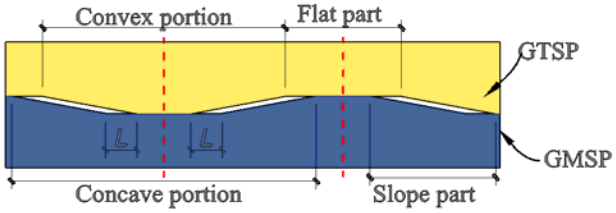

(a) The initial position of GTSP and GMSP

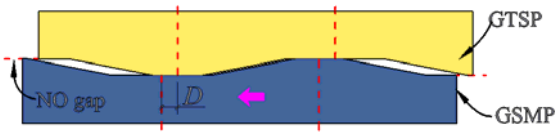

(b) $D < L$

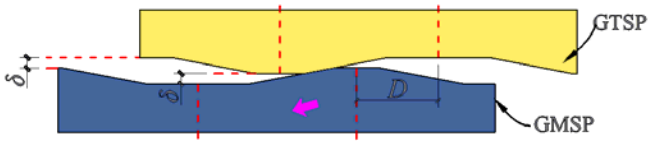

(c) $D > L$

Fig. 3 – The grooves of GTSP and GMSP

When the brace is in compressive states [Fig. 1 (b)] (i.e., the left end connection fixes and the right end connection moves leftward), right end connection moves to left direction together with inner tube, which pushes left end plate because right end connection is welded to right end of inner tube. Meanwhile, due to fixed left end connection, there is no movement in outer tube and right end plate. With the relative motion between inner tube and outer tube, some gaps occur between left end of outer tube and left end plate, between right end of inner tube and right end plate, causing relative movement between right end plate and left end plate. As the bolt system of BFRP tendons at end plates, BFRP tendons extend as same as end plates, generating an elastic resilient force against the relative movement between inner tube and outer tube and creating a tendency to return to the initial condition after loading, which achieves the self-centering function, too. Meanwhile, with the relative motion between inner tube and outer tube, the relative sliding frictions between GMSP and GTSP, between stainless plate and NAO pad will provide energy dissipation again.

When the brace is in tensile states [Fig. 1 (c)] (i.e., the left end connection fixes and the right end connection moves rightward), right end connection moves to right direction together with inner tube, which pushes right end plate because right end connection is welded to right end of inner tube. Meanwhile, due to fixed left end connection, there is no movement in outer tube and left end plate. With the relative motion between inner tube and outer tube, some gaps occur between right end of outer tube and right end plate, between left end of inner tube and left end plate, causing relative movement between right end plate and left end plate. As the bolt system of BFRP tendons at end plates, BFRP tendons extend as same as the end plates, generating an elastic resilient force against the relative movement between inner tube and outer tube and creating a tendency to return to the initial condition after loading, which achieves the self-centering function. Meanwhile, with the

relative motion between inner tube and outer tube, the relative sliding friction between GMSP and GTSP, between stainless plate and NAO pad will provide energy dissipation.

Therefore, with the process of tensile and compressive cycle deformations, pretensioned BFRP tendons provide continued self-centering force while VFD systems offer stable and expected energy dissipation in brace.

3. Prediction of SC-VFD Brace

3.1 The hysteresis curve of SC system

Based on the previous discussion, the working mechanism of SC-VFD brace is containing two parts: SC system and VFD system. Therefore, the hysteresis curve of SC-VFD brace is obtained by adding the hysteresis curve of SC system and VFD system.

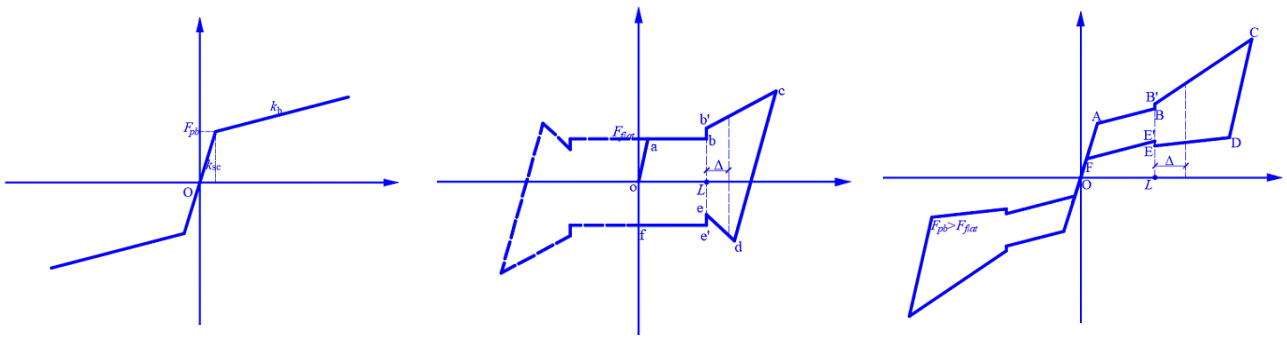

(a) SC system (b) two VFD systems (c) SC-VFD brace

Fig. 4 – Theoretical hysteresis curve of proposed SC-VFD system

As shown in Fig. 4(a), F_{pb} is pretension force in BFRP tendons, while k_{sc} is initial stiffness of self-centering system, containing stiffness of outer tube, k_{ou}, inner tube, k_{in} and BFRP, k_{bf}, respectively. When the inner tube and outer tube suffer from the F_{pb}, they generate some initial deformation and the length will become shorter. Thus, with increasing of external force, inner tube and outer tube have to conquer initial force in BFRP tendons. Therefore, the stiffness of BFRP in this stage is k_{sc}. After the SC system reach the pretension force in BFRP tendons, there are relative movements between inner tube and outer tube. Therefore, the stiffness of BFRP only contribute to the stiffness of SC system.

3.2 The hysteresis curve of VFD system

As shown in the Fig. 2 and Fig. 3, the friction forces of VFD systems are provided by two kinds of friction interface: between GTSP and GMSP with friction coefficients μ_s=0.16 [12] and between stainless plate and NAO pad with friction coefficients μ_d=0.33 [14]. Consider that when GTSP and GMSP, stainless plate and NAO pad suffer from relative movement, the force in VFD system can be calculated as

$$F_{flat} = 2 \times N_f \times n \times (\mu_s + \mu_d) \tag{1}$$

where N_f is the pre-stressing clamping forces applied to all friction bolts at both sides of VFD systems, n is the number of bolts at per side of VFD systems. Before the VFD system reach the sliding force, the stiffness of VFD system includes the stiffness of GTSP, GMSP, GBSP, stainless plate and NAO pad. After the external force reach the sliding force F_{flat}, the GTSP and GMSP, the stainless plate and NAO pad create some relative movement. Due to no deformation of disc spring

when $D < L$, the friction force keep as constant value, the stiffness of VFD system is 0. When the external displacement is larger than L, the combination of disc spring is compressed and the clamping force in bolts and the friction force between GTSP and GMSP, between stainless plate and NAO pad becomes larger.

The loading force analysis of GMSP and GTSP sliding at sloped part is shown in Fig. 5 (a). The normal force that is perpendicular to the slope, F_n, and friction force that is parallel to the slope, f, are developed and their expressions are depicted in Eq. (2).

(a) during loading stage (a) during unloading stage

Fig. 5 – Force analysis at slope part

$$\left.\begin{aligned} F_N \cos\theta &= f \sin\theta + N \\ F_N \sin\theta + f \cos\theta &= F_m / 2 \\ \mu_1 F_N &= f \end{aligned}\right\} \tag{2}$$

Using the principal force balance, loading force of GMSP and GTSP can be calculated as:

$$F_m = 2N \frac{\sin\theta + \mu_1 \cos\theta}{\cos\theta - \mu_1 \sin\theta} \tag{3}$$

Based on Eq.(3), sliding force of VFD systems at loading slope part F^l_Δ can be determined as:

$$\begin{aligned} F^l_\Delta &= 2 \times N_s \times n \times \left(\frac{\sin\theta + \mu_s \cos\theta}{\cos\theta - \mu_s \sin\theta} \right) + 2 \times N_s \times n \times \mu_d \\ &= 2 \times n \times \left(k\Delta \tan\theta + N_f \right) \times \left(\frac{\sin\theta + \mu_s \cos\theta}{\cos\theta - \mu_s \sin\theta} + \mu_d \right) \end{aligned} \tag{4}$$

Compared to stage a-b, sliding force at stage b′-c changes with different sliding distances, showing variable friction and post-yield stiffness.

Upon the unloading process, the stiffness k_{cd} is same as initial loading stiffness k_{oa} and sliding force at stage c-d changes into reverse direction. Then, as shown in Fig. 5 (b), unloading force of GMSP and GTSP at stage d-e can be calculated by Eq.(5), which is similar to loading stage.

$$\left.\begin{aligned} F_N \cos\theta &= f \sin\theta - F_b \\ F_N \sin\theta - f \cos\theta &= F_m / 2 \\ \mu_1 F_N &= f \end{aligned}\right\} \tag{5}$$

Likewise, using the principal force balance, unloading force of GMSP and GTSP can be calculated as:

$$F_m = 2N\frac{\sin\theta - \mu_1\cos\theta}{\cos\theta + \mu_1\sin\theta} \tag{6}$$

Similarly, based on Eq.(6), sliding force of VFD systems at unloading slope part F^u_Δ can be determined as:

$$\begin{aligned} F^u_\Delta &= 2\times N_s\times n\times\left(\frac{\sin\theta-\mu_s\cos\theta}{\cos\theta+\mu_s\sin\theta}\right)-2\times N_s\times n\times\mu_d \\ &= 2\times n\times\left(k\Delta\tan\theta+N_f\right)\times\left(\frac{\sin\theta-\mu_s\cos\theta}{\cos\theta+\mu_s\sin\theta}-\mu_d\right) \end{aligned} \tag{7}$$

Then, slip friction force always keeps constant as $-F_{flat}$ at stage e′-f until to compressive loading stage. Compared to stage e′-f, sliding force at stage d-e changes with different sliding distances, showing expected variable friction and post-yield stiffness.

3.3 The hysteresis curve of SC-VFD brace

Based on above analysis of SC-VFD brace mechanism, hysteresis curve of SC-VFD brace is formed by adding hysteresis curves of VFD systems and SC system, so does the stiffness. Consequently, the stiffness of SC-VFD brace at stage O-A k_{OA} is the summation of k_{sc} of SC system at first stage and k_{oa} of VFD systems at stage o-a. In addition, SC-VFD brace has to overcome the summation of sliding friction of VFD systems and pretension force of SC system to reach the sliding. So first activation force of SC-VFD brace F_A can be expressed as:

$$F_A = F_{flat} + F_{pb} \tag{8}$$

Similarly, besides stage O-A and F-O, the stiffness and force of other stages can be calculated as the summation of BFRP stiffness k_{bf} and stiffness of VFD systems at corresponding stages. Particularly, as same as stage O-A, the stiffness of SC-VFD brace at F-O stage k_{FO} is the summation of k_{sc} of SC system and k_{oa} of VFD systems.

In order to achieve self-centering function and capability, the force of SC-VFD brace at point F should be equal to or larger than 0, showing as:

$$F_{pb} > F_{flat} \tag{9}$$

If Eq.(9) cannot be satisfied, self-centering force in BFRP tendons would not overcome sliding force at point F during end of unloading process, showing unexpected residual deformation in brace.

4. Experiments and test result of SC-VFD Brace

4.1 Specimen Fabrication

As mentioned above, the length details of VFD systems seriously affect the loading ability of variable post-yield stiffness and energy dissipation, SC-VFD brace was designed. As shown in shown in Table 1, for a better understanding of SC-VFD brace mechanism, experiments of braces with same VFD systems but without BFRP tendons were also carried out. Therefore, Quasi-static experiments were carried out on all specimens using 1,000 kN hydraulic testing apparatus with maximum loading displacement of ±100 mm.

Table 1 – Parameters of SC-VFD braces and VFD braces

Specimen		Specimen I	
		SC-VFD	VFD
SC system	Number of BFRP tendons	2	NONE
	Pretension force of each BFRP (kN)	35	
	Initial deformation of BFRP (mm)	6.3	
VFD systems	Flat distance (mm)	7	
	Slope distance (mm)	21	
	Height of slope part (mm)	4	
	tan θ (θ is the angle of grooves)	0.190	
	Disc Springs in parallel	4	
	Disc Springs in series	5	
	Force capacity of disc springs in per bolts (kN)	48	
	Pre-stressing force in the bolts (kN)	16	
	Sliding force at flat part (kN)	47.0	

4.2 Test results

As mentioned above, in order to get better understanding of SC-VFD braces, braces without BFRP, called VFD braces were carried out and the hysteresis curves of VFD brace are shown in Fig. 6(a) and stiffness of VFD brace is shown in Table 2. Similar to theoretical hysteretic curve, obvious corner points and different post-yield stiffness can be observed in hysteresis curve of VFD brace in Fig. 6(a). Before VFD brace slides at slope part [Fig. 6(a)], it's similar to BRB braces or other friction dampers, which only have one activation and constant stiffness (k_{ab}) after activation. The second activation of VFD brace is achieved at end of flat part, which is ±7mm [Fig. 6(a)], with larger friction, post-yield stiffness (k_{bc}) and energy dissipation as expected. This result is called variable friction. Although abrupt increasing and decreasing at ±7mm during loading stage are not obvious as theoretical analysis, the force of VFD brace still shows gradually increasing and catches up with theoretical data at distance 10 mm in tension or -10 mm in compression approximately. While during unloading stage, the abrupt increasing and decreasing at ±7mm are more obvious and consume only 1mm to catch up with theoretical data. Therefore, test result of VFD brace depicts same tendency with theoretical analysis, meaning proper working of VFD brace.

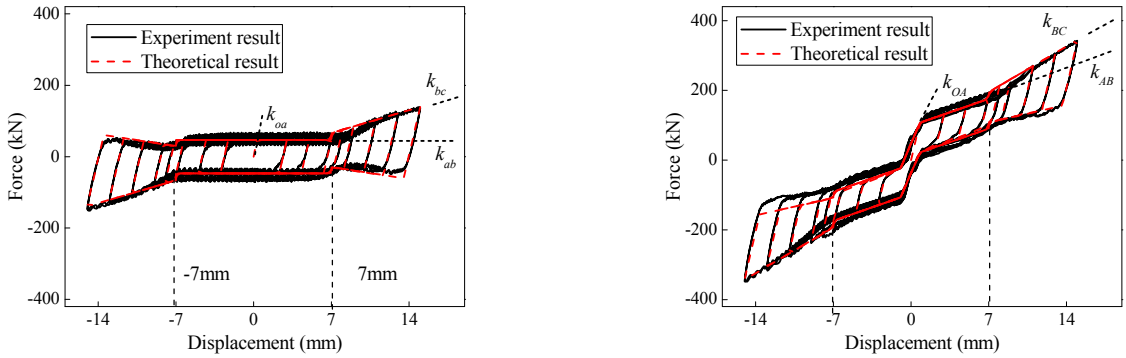

(a) VFD brace (b) SC-VFD brace

Fig. 6 – Hysteresis curve of Specimen

Table 2 – The stiffness of Specimen (Unit: kN/mm)

Specimen		k_{oa} (k_{OA})	k_{ab} (k_{AB})	k_{bc} (k_{BC})
VFD	Theoretical analysis	162.79	0	9.20
	Experimental result	151.04	0	9.63
SC-VFD	Theoretical analysis	134.15	11.01	20.21
	Experimental result	129.32	10.45	19.87

As shown in Table 1, sliding force of VFD systems at flat part is calculated as 47.0 kN in theory and pretension force of total BFRP is 70 kN as measured, which is larger than sliding force of VFD systems. Thus, the brace can provide sufficient restoring force and achieve self-centering function in theory. The stiffness of SC-VFD brace at each stage is shown in Table 2 and hysteresis curves of SC-VFD brace, as shown in Fig. 6(b), depict a variable flag shape hysteresis curve, showing self-centering phenomenon. Meanwhile, like VFD brace, abrupt increasing and decreasing at ±7 mm during loading stage is not clear while during unloading stage, abrupt changing is more obvious. Furthermore, before SC-VFD slides at slope part [Fig. 6(b)], the hysteresis curve is similar to the original SC-BRB or other SC-FD, exhibiting only one activation, two different stiffness (k_{OA} and k_{AB}) and normal flag shape. In the hysteresis curve of SC-VFD with a larger sliding distance after ±7 mm, which is end of flat part [Fig. 6(b)], there are two obvious corner points and three different stiffness (k_{OA}, k_{AB} and k_{BC}) in each cycle of loading or unloading stage, presenting larger friction, post-yield stiffness (k_{BC}) and energy dissipation as expected. This phenomenon is called variable friction. Also, the stiffness of SC-VFD brace at second and third stage is summation by stiffness of VFD brace and BFRP tendons approximately.

With incensement of external displacement, although residual deformation is very small, but still exists. When external load displacement reaches 14 mm in tension, known as the 2% drift, residual displacement is 0.45 mm, while when external load displacement reaches -14 mm in compression, residual displacement is 0.75 mm, which is bigger than residual displacement in tension. The average residual deformation after maximum load is no exceeded 0.1% drift. Although residual displacement increases slightly, test results still present a fine variable flag shape, meaning the proper working of SC system.

However, although considering influence of the tube length tolerance, compared to theoretical data, the experimental stiffness of first loading stage is still smaller than theoretical analysis and SC-VFD still exists little residual displacement. It's mainly because of some assembly gap between brace and hydraulic testing apparatus, end connections and attachment plates, different lengths of inner tube and outer tube due to manufacturing and fabrication, and welding imperfections in all parts of SC-VFD.

5. Conclusion

In this paper, a novel self-centering energy dissipation brace is mentioned and developed. Based on the experiential and theoretical analysis, ysteresis performance of VFD braces and SC-VFD braces are performed, and the results are presented below:

1 The experimental result and theoretical analysis considering the influence of tube length tolerance of VFD braces and SC-VFD braces show same tendency.

2 The hysteresis curves of SC-VFD braces in quasi-static experiments show a normal flag-shape behavior at flat part while hysteresis curves show variable flag-shape with another activation,

sliding force and post-yield stiffness at slope part under different sliding distances, which can provide sufficient energy dissipation capacity.

3 Residual displacements of braces are smaller than 0.1% drift, demonstrating expected self-centering phenomenon under cyclic loading protocols.

6. Acknowledgements

The authors would like to acknowledge financial supports from “National Key Research and Development Program of China” (2018YFC0705700), “National Natural Science Foundation of China” (51878150).

7. Copyrights

8. References

[1] GIUGLIANO M T, LONGO A, MONTUORI R, et al. Plastic design of CB-frames with reduced section solution for bracing members (2010). *Journal of Constructional Steel Research,* 66(5): 611-21.
[2] AIKEN I D, NIMS D, KELLY J M. Comparative study of four passive energy dissipation systems (1992). *Bulletin of the New Zealand National Society for Earthquake Engineering,* 25(3): 175-92.
[3] AIKEN I D, NIMS D K, WHITTAKER A S, et al. Testing of passive energy dissipation systems (1993). *Earthquake spectra,* 9(3): 335-70.
[4] XIE Q, ZHOU Z, MENG S-P. Experimental investigation of the hysteretic performance of self-centering buckling-restrained braces with friction fuses (2020). *Engineering Structures,* 203(1): 109865.
[5] ZHOU Z, XIE Q, LEI X, et al. Experimental investigation of the hysteretic performance of dual-tube self-centering buckling-restrained braces with composite tendons (2015). *Journal of Composites for Construction,* 19(6): 04015011.
[6] ZHOU Z, XIE Q, MENG S, et al. Hysteretic performance analysis of self-centering buckling restrained braces using a rheological model (2016). *Journal of Engineering Mechanics,* 142(6): 04016032.
[7] RODGERS G W, SOLBERG K M, CHASE J G, et al. Performance of a damage‐protected beam–column subassembly utilizing external HF2V energy dissipation devices (2008). *Earthquake Engineering & Structural Dynamics,* 37(13): 1549-64.
[8] QIU C-X, ZHU S. High-mode effects on seismic performance of multi-story self-centering braced steel frames (2016). *Journal of Constructional Steel Research,* 119(1): 133-43.
[9] HASHEMI A, YOUSEF-BEIK S M M, DARANI F M, et al. Seismic performance of a damage avoidance self-centring brace with collapse prevention mechanism (2019). *Journal of Constructional Steel Research,* 155(3): 273-85.
[10] HASHEMI A, ZARNANI P, MASOUDNIA R, et al. Seismic resistant rocking coupled walls with innovative Resilient Slip Friction (RSF) joints (2017). *Journal of Constructional Steel Research,* 129(4): 215-26.
[11] LI C, XUE Y. Experiment and Analysis on the Performance of" Spring-Slope" Variable Friction Dampers (2013). *Building Science,* 29(3): 34-9.
[12] HASHEMI A, MASOUDNIA R, QUENNEVILLE P. A numerical study of coupled timber walls with slip friction damping devices (2016). *Construction and Building Materials,* 121(3): 373-85.
[13] HUANG L J, ZHOU Z, HUANG X G, et al. Variable friction damped self-centering precast concrete beam–column connections with hidden corbels: Experimental investigation and theoretical analysis (2020). *Engineering Structures,* 206(1): 110150.
[14] HUANG X G, ZHOU Z, XIE Q, et al. Seismic Analysis of Friction-Damped Self-Centering Coupled-Beams for Moment-Resisting-Frames without Floor Elongation (2018). *Journal of Earthquake and Tsunami,* 12(05): 1850012.

